Reversible motions and disordered structure of soft particles in amorphous solids

Xinyu Fan,[1,2] Cai-Zhuang Wang,[3,*] Kai-Ming Ho,[3] M. S. Altman,[2] and Li Huang[1,†]

[1]*Department of Physics, Southern University of Science and Technology, Shenzhen, Guangdong 518055, China*

[2]*Department of Physics, Hong Kong University of Science and Technology, Clear Water Bay, Kowloon, Hong Kong SAR, China*

[3]*Ames Laboratory, U.S. Department of Energy and Department of Physics, Iowa State University, Ames, Iowa 50011, USA*

(Received 12 September 2021; accepted 8 March 2022; published 21 March 2022)

In amorphous solids, soft vibrational modes derived from normal mode analysis can be utilized to identify the soft particles that are prone to irreversible rearrangements. However, the normal mode analysis approach cannot explain why the spatial distributions of clustered soft particles do not change over time. We define a softness parameter based on the vibrational density of states calculated directly from molecular dynamics simulations with both the harmonic vibrations and anharmonic relaxations being properly captured at finite temperatures. This parameter spontaneously correlates with the real space atomic motions and the dynamics heterogeneity. Using the softness parameter, we show that the softest particles are confined within rigid cages. These particles keep rearranging reversibly without long-range diffusion. The moderately soft particles rearrange irreversibly, and the hard particles mainly participate in vibrations without rearrangement. We also show that the soft particles form locally disordered structures, while the hard particles present strong ordering. These findings confirm the defective nature of soft particles, and provide insights on the nature of softness as the ability to rearrange, but not necessarily irreversibly.

DOI: 10.1103/PhysRevB.105.104112

I. INTRODUCTION

Defective sites in crystalline solids can be defined in terms of the deviations from the ideal long-range periodicity of a given lattice. One important property of the defects is that they can serve as precursors of structural rearrangement. Since the disordered structure in amorphous solids hinders the identification of structural defects, it is not clear whether structural defects in amorphous systems can even be defined [1,2]. The ambiguity of the nature of defects makes the quantification of defect-related properties in amorphous solids extremely hard. For example, the prediction of atomic rearrangement remains one of the central challenges in glass science. Numerous efforts have been devoted to studying the physics of structural defects in amorphous solids on a general basis, some of which are from atomic a topology perspective [1,3–5], while others focus on the potential energy landscape (PEL) aspect [6–10]. In recent years, several approaches based on machine-learning algorithms have been developed to address this longstanding challenge that have provided new insights into the relationship between structure and dynamics in glasses [11–13].

Among the various indicators, the particles participating in the quasilocalized low-frequency normal modes [14–17], usually termed as soft particles, are strong candidates for flow defects [18] and exhibit a high propensity for motion [19] in glassy systems. The soft particles are plastically unstable, which means they can have large nonaffine displacements when subjected to athermal quasistatic shear deformation [17]. The atomic softness can be estimated by summing up the participation fractions of the lowest vibrational modes, which characterizes the tendency to rearrange and the flatness of energy basins [19–21]. Despite these understandings, there are still several questions left unanswered for soft particles. A recent study shows that the particles with high atomic softness evaluated using very soft modes are plastically unstable, while the particles with high softness obtained from less soft modes are prone to irreversible rearrangement instead [22]. The different behaviors of soft and very soft particles cause confusion on the nature of atomic softness, as well as the properties of the potential defects. Another question is related to the dynamics of the soft particles. While it was shown that the soft particles rearrange irreversibly under strain or thermal activation, little change is observed for the clustering of soft particles (soft region) [21,23]. It is thus necessary to explore the relationship between atomic softness and real space atomic motions. A more fundamental question is about the structural signature of the soft particles. Recent works found that the local structures of soft particles can be characterized by geometrically unfavored motifs [5] and are surrounded by solidlike regions [24]. Unfortunately, a more explicit description on their local structures is still absent [2,11,25]. While the soft spots have local environments very different from the dominant short-range order (SRO) [5,15,26], do they possess other types of orders or are they totally disordered? Answers to these questions are crucial for unveiling the physical nature of atomic softness and defects in amorphous solids, which may further clarify the structure-dynamics relationship in amorphous solids.

A commonly adopted approach to determine the soft vibrational modes is to diagonalize the dynamic matrix (DM)

*Corresponding author: wangcz@ameslab.gov

†Corresponding author: huangl@sustech.edu.cn

derived from the inherent structures of glass samples after energy minimization at 0 K. With the harmonic approximation, the normal mode analysis is supposed to provide the information about the profiles of the bottom of potential energy basins, and the soft modes represent directions to escape from the basins with least effort [25]. However, the cage-breaking relaxations, both strain and temperature triggered, are barrier-crossing events with strong anharmonicity [1,7,27,28]. A new softness parameter with the anharmonic properties being properly included is thus desirable to establish the correlation between atomic softness and real space motions.

In this paper, we show that, with both the harmonic vibrations (in-cage motions) and anharmonic relaxations (cage-breaking hops) being properly captured at the same time, the soft particles can be identified based on the vibrational density of states (VDOS) directly obtained from molecular dynamics (MD) simulations (MD-VDOS). A new softness parameter is also proposed, which can be explicitly related to the particle motions, akin to other order parameters that incorporate dynamical information [18,29]. By scrutinizing the trajectories of atoms with different softness, we find that the softest particles keep rearranging reversibly, while the particles undergoing nonreversible rearrangements do so at a lower rate than the softest particles and are thus moderately soft. Furthermore, particles mainly undergoing harmonic motions are the hardest, and therefore barely contribute to the low-frequency intensity in MD-VDOS. Structural analysis shows that soft particles have essentially disordered local environments, while hard particles have well-developed order. These findings confirm the defective nature of soft particles, and provide insights into the nature of softness as the ability to rearrange, but not necessarily irreversibly.

II. METHODS

We choose a well-studied binary glass-forming Lennard-Jones system, the Kob-Andersen (KA) model [30], as a representative of amorphous solids. This system has the composition of $A_{80}B_{20}$, where A and B correspond to the larger and smaller particles, respectively, interacting with each other via the Lennard-Jones potential with the following parameters: $\epsilon_{AA} = 1.0$, $\epsilon_{BB} = 0.5$, $\epsilon_{AB} = 1.5$, $\sigma_{AA} = 1.0$, $\sigma_{BB} = 0.88$, and $\sigma_{AB} = 0.8$, the same as in the original paper and our previous work [31]. A smooth cutoff scheme is adopted, in which both energy and force go continuously to zero at the cutoff distance of $2.5\sigma_{AA}$ [32]. To explore the effects of system size, three system sizes with the number of atoms N being 500, 4000, and 8000 are considered. Periodic boundary conditions are applied in all directions. The MD simulations are carried out using the LAMMPS package [33], with the isothermal-isobaric ensemble (N-P-T) through the Nosé-Hoover thermostat. The box sizes are allowed to relax during the simulations so that the pressure is kept zero. The systems are first equilibrated at a high temperature well above the glass transition temperature (T_g), then cooled down to the desired temperature using a constant cooling rate of 1×10^{-5}. The time step is set to $2 \times 10^{-3}\tau$, where τ is the Lennard-Jones time unit. The frequency is in units of $2\pi/\tau$. In the remainder of the description of the work, all the quantities are reported in reduced Lennard-Jones units for clarity.

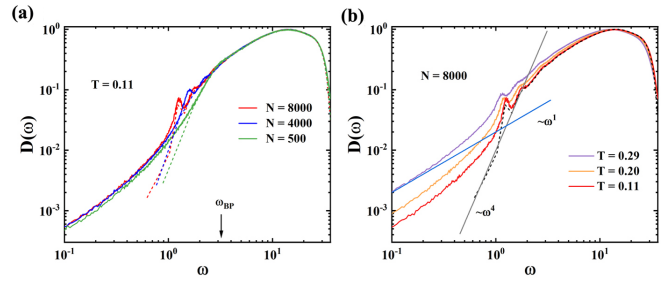

FIG. 1. (a) The comparison between DM-VDOS and MD-VDOS for systems with different sizes at $T = 0.11$. (b) The MD-VDOS for KA glasses at different temperatures, with the DM-VDOS as a reference. The DM-VDOSs are shown with dashed lines, while the MD-VDOSs are indicated by solid lines. As the DM-VDOS does not change much in the glass state, we only present the DM-VDOS at $T = 0.11$. Two eye-guiding lines with different slopes are included. The VDOSs are scaled so that their maxima equal to unity. The DM-VDOSs at different temperatures are calculated using the inherent structures of the glass at the corresponding temperatures.

To capture the anharmonic relaxations at finite temperatures, the MD-VDOS is obtained by taking the Fourier transform of velocity autocorrelation functions [16,34–36], instead of the more commonly adopted dynamic matrix method (DM-VDOS) within the harmonic approximation. By making use of the per-atom nature of the velocity autocorrelation functions, the MD-VDOS method has been adopted in previous studies to identify the particles with high boson peak (BP) intensities [37–41]. The velocity autocorrelation function of each particle is calculated by

$$C_i(t) = \frac{\sum_{t_0} \boldsymbol{v_i}(t+t_0)\cdot\boldsymbol{v_i}(t_0)}{\sum_{t_0} \boldsymbol{v_i}(t_0)\cdot\boldsymbol{v_i}(t_0)},$$

where $\boldsymbol{v_i}(t)$ is the atomic velocity at time t and t_0 is the initial time moment. Then, the per-atom VDOS can be computed by the time Fourier transform:

$$D_i(\omega) = \int_{-\infty}^{+\infty} C_i(t) e^{j\omega t} dt = 2\int_0^{+\infty} C_i(t)\cos(\omega t) dt.$$

The sum of per-atom VDOS then yields the total VDOS. As the velocity autocorrelation function is essentially based on a convolution operation, we can further reduce the computational load by applying the convolutional theorem:

$$D_i(\omega) = \sum_{\alpha=x,\,y,\,z} \mathcal{F}\left(v_i^\alpha * v_i^\alpha\right) = \sum_{\alpha=x,\,y,\,z} \mathcal{F}\left(v_i^\alpha\right)\mathcal{F}\left(v_i^\alpha\right),$$

where $\mathcal{F}$ and $*$ denote the Fourier transform and convolution operations, respectively. By calculating the proportion of individual particles' VDOS to the overall MD-VDOS, we can easily identify the particles with the largest contributions to the low-frequency intensity. More details about how the MD-VDOS is obtained can be found in the Supplemental Material [42].

III. RESULTS AND DISCUSSIONS

In Fig. 1(a), we compare the MD-VDOS and the DM-VDOS for KA glasses with different system sizes. One can see from Fig. 1 that for all sizes considered, the MD-VDOS and

DM-VODS coincide with each other in the high-frequency region. However, in the low-frequency side, noticeable discrepancies emerge. Recent works show that the $D(\omega) \sim \omega^4$ law at low-frequency regime persists even at finite temperatures if the SRO cages are well preserved [43,44]. Thus, the deviation from ω^4 law in the MD-VDOS may originate from the cage-breaking motions. Overall, the MD-VDOS show richer low-frequency components compared to that of DM-VDOS, and the deviation starts from the BP frequency, as indicated by the arrow. The peaks of Goldstone modes can be clearly seen in the MD-VDOS for $N = 4000$ and 8000 systems, which also appear in DM-VDOS for $N = 8000$. We show in the Supplemental Material that these phonons barely affect the identification of soft particles [42]. As the frequency decreases, the MD-VDOS for different system sizes coincide again. The DM-VDOS of systems with different sizes are essentially identical in the high-frequency region, while the low-frequency components decrease with the system size, which agrees with previous reports [16,45,46].

In Fig. 1(b), we show the VDOS at several temperatures for the $N = 8000$ system. As revealed by our previous study, the T_g of the KA system at this cooling rate is around 0.32 [31]. Since the DM-VDOS is derived from the inherent structures, which barely change for $T < T_g$ [47,48], only the DM-VDOS at $T = 0.11$ is presented. Again, the DM-VDOS and MD-VDOS match well in the high-frequency region for all temperatures. As the temperature decreases, the MD-VDOSs shift toward higher frequencies. Performing the evaluation at lower temperature also results in a diminished low-frequency ($\omega < \omega_{BP}$) component in the MD-VDOS, and a smaller difference with the DM-VDOS. The dependence of the low-frequency intensities on the sampling time and temperature of low-frequency intensity suggests that they may originate from the relaxations. We find that the low-frequency end of the MD-VDOS at $T = 0.29$ approaches ω^1, implying that the $D(\lambda = \omega^2)$ is nearly constant for λ close to or even smaller than zero. The effect of unstable modes is thus evaluated in the Supplemental Material [42]. As expected, the unstable modes emerge for $T = 0.20$ and above. Our results suggest that the high-frequency vibrations in KA glass are mainly harmonic, while the low-frequency modes are dominated by the anharmonic effect governing the relaxations [1,27,28,49,50].

We now illustrate how to define the softness parameter based on the MD-VDOS. The softness parameter is defined by measuring the contribution of the ith particle's VDOS to the global VDOS in the low-frequency range:

$$S(i) = \sum_{\omega<\omega_c} \frac{D_i(\omega)}{\sum_i D_i(\omega)},$$

where the $D_i(\omega)$ is the VDOS of the ith particle, and the summation goes up to some cutoff frequency (ω_c). A rule of thumb in the normal modes analysis approach for identifying the soft particles is to sum the participation fractions of the 0.5%–1% eigenmodes with the lowest frequencies [19,21,25]. We follow the same methodology to get the softness parameter S. By varying the upper and lower bounds of cutoff frequencies, S can be used to project the VDOS within other frequency regions to individual particles. In Fig. 2(a), we present the total VDOS (upper panel) and the individual

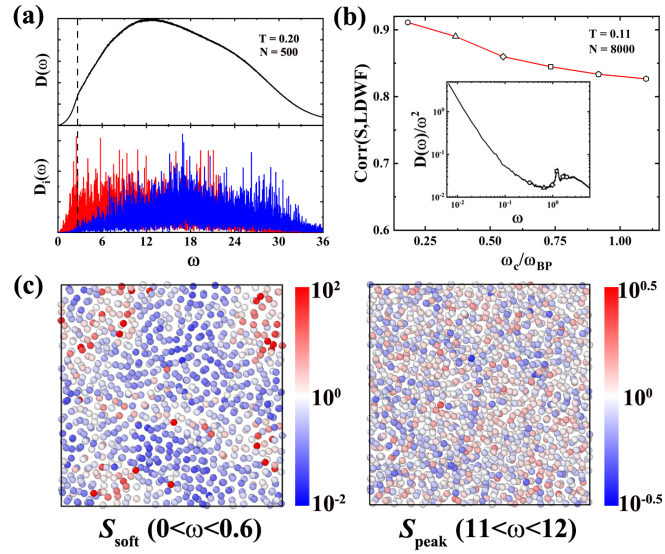

FIG. 2. (a) The total VDOS (upper) and the VDOS for the particle with largest (lower, red) and smallest (lower, blue) contribution to the low-frequency intensities in MD-VDOS. The dashed line indicates the boson peak frequency. (b) The Pearson correlation coefficient $\frac{\sum(A_i-\bar{A})(B_i-\bar{B})}{\sqrt{\sum(A_i-\bar{A})^2}\sqrt{\sum(B_i-\bar{B})^2}}$ (A and B are different observables) with local Debye-Waller factor for S obtained using different ω_c. (c) The spatial distribution of S calculated from different frequency regions. S is scaled using the system average before performing the color coding; a slab with thickness of 2 is adopted. (c) is visualized using the OVITO package.

VDOS of the softest and hardest particle identified using S (lower panel). The two particle-level VDOSs show an obvious difference in the low-frequency region, indicating the ability of S to identify the soft particles. In Fig. 2(b), we illustrate the Pearson correlation coefficient between S and the local Debye-Waller factor (LDWF), a parameter that has been proven to be highly correlated with the dynamic heterogeneity, the soft modes, plastic instability, and activation energy [25,29,51]. The LDWF of each atom is defined as $\alpha_i = \langle[r_i(t) - r_i(0)]^2\rangle$, where r_i is the position of particle i sampled every 1τ until the maxima simulation time, and $\langle\cdots\rangle$ denotes averaging over the collected atomic positions. Different ω_c are chosen to test the robustness of S. The hereby obtained softness parameter is highly correlated with the LDWF, and the correlation rarely changes with ω_c. It is also interesting to note that the highest correlation appears at the lowest ω_c, at which the reduced VDOS diverges [see the inset of Fig. 2(b)], implying the importance of anharmonic relaxations [27,41]. Here we choose a temperature as low as $1/3\ T_g$ to monitor the relationship between S and LDWF in Fig. 2(b), and the simulation time is well below the relaxation time (see Fig. S2 in the Supplemental Material [42]). The good correlation between S and LDWF demonstrates the S's ability to describe pure vibrations. As we increase the temperature or simulation time, the LDWF can no longer be calculated due to the emergence of more complex dynamics such as rearrangement. In that case, S is still capable of distinguishing different dynamics, as will be illustrated later. In Fig. 2(c), we present each particle's contribution to the soft-region (S_{soft}, $0 < \omega < 0.6$) and the peak-region intensities

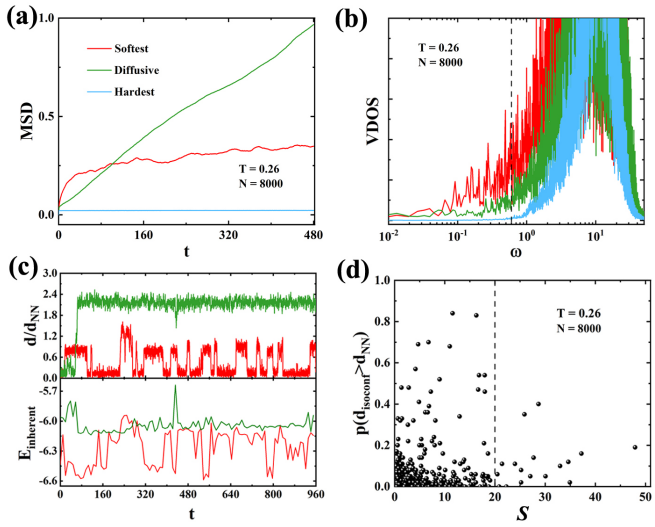

FIG. 3. (a) The MSD of the particles with the largest S_{soft} (red), the largest displacement (green), and the largest S_{peak} (cyan). (b) The corresponding VDOS for the three groups of atoms in (a). (c) The normalized displacement, d/d_{NN} (upper), and the inherent energy, E_{inherent} (lower), as a function of time for two particles with the largest softness (red) and displacement (green), respectively. To collect the particle's energies in their inherent states, 100 configurations are sampled every 9.6τ during the MD simulations and then minimized to their inherent states using a combination of FIRE and conjugate gradient method implemented in LAMMPS [33]. (d) The probability of having a displacement larger than the nearest neighbor distance at the end of each isoconfigurational run for each particle. The dashed line indicates the cutoff softness for reversible rearrangements.

(S_{peak}, $11 < \omega < 12$), respectively, at $T = 0.26$. S_{soft} and S_{peak} are scaled using the system averages before implementing the color coding in the figures. Different color scales are adopted so that the spatial heterogeneities of both frequency regions can be better recognized. The particles with significant contributions to the soft-region vibrations exhibit strong clustering spatial distribution, while the spatial heterogeneity of the particles contributing the peak-region intensities is clearly much weaker even with a narrower color scale. These results are in accordance with the spatial distribution from the normal mode analyses [19,26,49], which, together with the good correlation between LDWF and S, suggest that S_{soft} is equivalent to the softness parameter based on the normal mode analyses [1,14–16,26,52]. Furthermore, the real space motions of the particles contributing to the low-frequency components in MD-VDOS can be tracked easily, which makes it possible to explore the direct connection between softness and the dynamics of particles. We use the softness parameter calculated using $\omega_c = 0.6$ in the remaining part of this work.

Next, we compare the mean square displacement (MSD) and average VDOS of particles from different groups, i.e., the top 0.5% particles with largest displacement (diffusive), and the same number of particles with largest S_{soft} and S_{peak}, in Fig. 3. Increasing the number of particles does not qualitatively alter our results (see Fig. S5 in the Supplemental Material [42]). To remove the noise, we compute the MSD by averaging over atomic displacements as well as the initial positions:

$$\text{MSD}(t) = \frac{1}{N}\langle[\boldsymbol{r}_i(t+t_0) - \boldsymbol{r}_i(t_0)]^2\rangle_{t_0},$$

where $\boldsymbol{r}_i$ is the position of particle i, N is the number of particles, and t and t_0 range from zero to half of the maxima MD simulation time. We can see from Fig. 3(a) that the peak particles are mainly participating in harmonic vibrations around their original positions, as illustrated by the flat MSD with small amplitude. On the other hand, the MSD amplitude of the diffusive particles at $t = 480\tau$ is close to 1, which is larger than the nearest neighbor distance ($d_{\text{NN}} = 0.9$) in KA glass [31], implying that the diffusive particles rearrange irreversibly during the MD simulation. In contrast to the other two groups of particles, the MSD of the softest particles saturates at a plateau very soon, which suggests that the dynamics of the softest partcicles is more complex than pure vibration or diffusion. A previous study suggested that the vibrational eigenfrequency can abruptly drop toward zero in the limit of atomic rearrangement [15]. We also observe a strong dependence of the low-frequency intensity in MD-VDOS on sampling time and temperature, suggesting that our softness parameter may be closely related to relaxation dynamics [42]. In Fig. 3(b), we show that the different relaxation behaviors of the particles can distinguish them in the low-frequency region in the MD-VDOS. One can see from Fig. 3(b) that the softest (peak) particles show very rich (poor) low-frequency intensities in their MD-VDOS. The peak particles can thus be regarded as hard particles, while the diffusive particles undergoing irreversible rearrangements exhibit intermediate softness compared to the other two groups.

Knowledge on the displacement of individual particles is needed to fully understand the relationship between atomic dynamics and softness and the physical meaning of our softness parameter, which is also helpful to understand the persistence of the soft region over time [21,23]. In the upper part of Fig. 3(c), we compare the displacement of the softest particle and the most diffusive particle as a function of time, and their energies in the corresponding inherent states are displayed at the bottom of Fig. 3(c). Here 100 configurations are sampled at a time interval of 9.6τ during the MD simulations, then optimized to their inherent states through energy minimization [53] using a combination of fast inertial relaxation engine (FIRE) and conjugate gradient (CG) algorithm implemented in LAMMPS [33]. We can see in Fig. 3(c) that the particle's inherent energy without the thermal noise can serve as an indicator of basin hopping or rearrangement. The displacements are in units of $d_{\text{NN}} = 0.9$, which is the nearest distance between the B particle and the A particle [31], and is large enough to break the nearest neighbor cage [54–56]. An apparent character of the motion of the softest particle is the surprisingly large displacement amplitude, often close to or even larger than d_{NN}. However, breaking the nearest neighbor cage does not necessarily lead to irreversible rearrangement. The softest particle is obviously hopping reversibly among several distinct positions without long-range diffusion, resulting in its unique MSD in Fig. 3(a). The reversible hopping with large displacement amplitude suggests that the very soft particles undergo relaxations with mixed vibrations and rearrangements within a rigid cage larger than

the SRO. Similar reversible motions have been observed in other systems and are related to the secondary relaxation and boson peak [41,57,58]. In contrast, the particle with the largest displacement reaches a relatively stable position after several smaller stepwise jumps, indicating an irreversible rearrangement. By associating the softness with an individual particle's trajectory, one can see that S correctly identifies particles with distinctly different dynamics, i.e., diffusive, vibratory, and mixed rearranging-vibratory motions. Thus, compared to LDWF that focuses on short-time vibrations, S can better reflect the dynamics heterogeneities over longer timescales.

It can be seen in Fig. 3(c) that particle rearrangements are accompanied by a sudden change of the inherent energy. Therefore, we can define the number of basin-hopping events a particle experiences as $n_{\rm hop} \sim \sum_{t=0}^{t_{\rm max}} |\Delta E_{\rm inherent}|$, where $\Delta E_{\rm inherent}$ is the difference between a particle's energy in the inherent states at adjacent time moments. The summation over many time moments makes $n_{\rm hop}$ focus more on the overall rearranging rate, instead of one single jump. If there is no basin hopping during the MD simulation, $n_{\rm hop}$ is equal to zero and the corresponding $\Delta E_{\rm inherent}$ would be close to zero all the time. If the particle rearranges frequently, then the accumulated $|\Delta E_{\rm inherent}|$ would be large. For the top 0.5% softest particles, the average $n_{\rm hop}$ is around 11, while for the top 0.5% most diffusive particles, this value is around 7 and the system average is about 1.6. The origin of the rich low-frequency intensity in the MD-VDOS can thus be considered to arise from the barrier-crossing relaxations. In this regard, one can say that an atom becomes softer when it experiences more basin-hopping events. Our softness parameter thus measures the ability to rearrange, just like the softness defined from the normal mode analyses [19–21]. However, unlike the previous studies focusing on the bottom of each energy basin only, the MD-VDOS approach profiles both the current and neighboring energy basins in the PEL, and the shapes of the neighboring basins determine whether one particle can keep rearranging or not when it jumps.

Since one particle trajectory only provides one sampling of the propensity for motion [59], we also perform the isoconfigurational ensemble simulations to establish the correlation between S and rearrangements. The time interval for each isoconfiguration run is chosen to be the time interval adopted in MD simulations, $t = 960\tau$. After performing 100 isoconfigurational runs, we calculate the probability of having a displacement larger than $d_{\rm NN}$ at $t = 960\tau$ for each particle, as illustrated in Fig. 3(d). The particles with high tendency to jump out of the cage usually have moderate S, while probabilities of breaking the nearest neighbor cages for the softest particles (S>20) and hardest particles are small, in qualitative agreement with Fig. 3(a). Combining Fig. 2(c) and Fig. 3, one can conclude that the softest particles are hopping reversibly within a large space formed by the hard particles, which explains why the soft regions can survive many rearrangements [21,23]. More importantly, we show that the soft particles may not exhibit a high propensity for irreversible motion.

A fundamental question left unanswered concerns the structural signature of the soft particles: are they totally disordered, or do they share some order different from the dominant SRO? Firstly, we check whether the soft particles are loosely packed or not by calculating their atomic stresses,

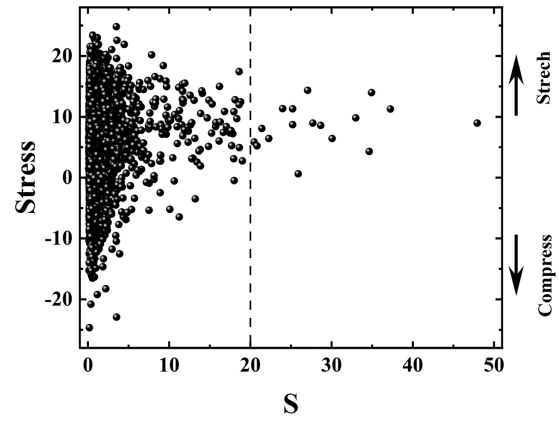

FIG. 4. The atomic stresses as a function of softness. The atomic stresses are calculated by averaging the configurations sampled within 2τ in time intervals of 0.02τ. The dashed line indicates the cutoff softness for reversible rearrangements.

as illustrated in Fig. 4. The atomic stresses are obtained by averaging the diagonal elements of the stress tensor. Overall, the softness does not correlate well with the atomic stress. Nevertheless, it can be seen that the softest particles are indeed in slightly stretched states, in agreement with previous reports [1,10,12,15,39].

To obtain a more quantitative description on the structure of the soft particles, we employ the cluster alignment method to characterize the atomic structures [60–63]. In our previous work, we show that the SRO can be identified based on pairwise cluster alignment and clique analysis [31]. The pairwise alignment method measures the similarities between each cluster and all the other clusters; the smaller the alignment score, the higher the similarity. The resulting similarity matrix can then be used to identify the cliques (groups of clusters sharing similar atomic packing motifs) by applying the clique analysis [60,61]. The sizes and number of cliques that are identified reflect the degree of ordering. We choose the top 5% B particles with the largest $S_{\rm soft}$ and $S_{\rm peak}$ to perform the pairwise cluster alignment, as both the SRO and medium-range order (MRO) in KA glass are B-centered clusters. The similarity matrices of the two groups of B particles after clique analysis are shown in Fig. 5(a). The distribution of pairwise alignment scores is also shown in Fig. S6 in the Supplemental Material [42]. It can be seen that the cluster distortion of the soft particles is much larger than that of the hard particles. To save some computational cost, we adopt a more rigorous cutoff score (0.10) during the clique analysis. As suggested by the small number of cliques and tiny sizes, the local environments of the soft particles do not resemble each other. In contrast, a number of cliques with significantly larger sizes can be identified among the hard-particle-centered clusters even with a very rigorous cutoff score, implying their strong ordering. By monitoring the geometric structures of clusters within cliques for both soft and hard particles, we find that the packing motif shared by the clusters is the same as the dominant SRO in the KA model [31]. We then align the clusters with the dominant SRO and MRO in KA glass, whose structures are shown in the insets of Fig. 5(b). Roughly 16% of the soft particles have well-developed SRO,

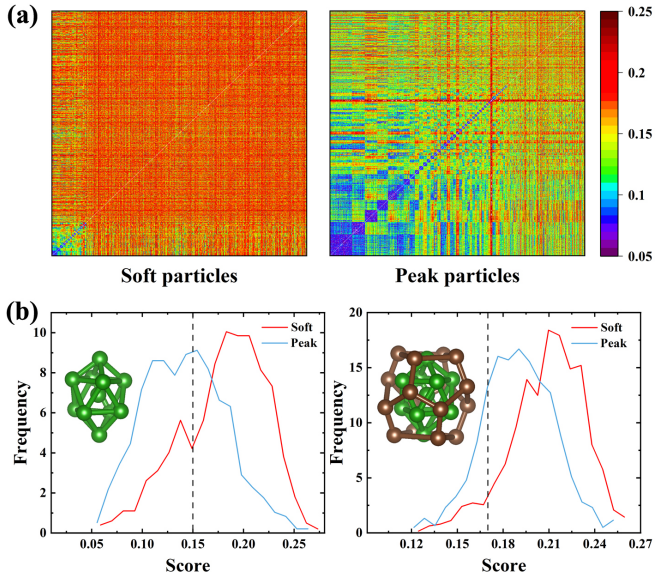

FIG. 5. (a) The similarity matrices of 5% B particles contributing the most to the soft-region intensities of the MD-VDOS (left) and peak-region intensities (right) after clique analysis. Each pixel is an alignment score between the ith and jth cluster. (b) The distribution of alignment scores for soft (red) and peak (blue) particles against SRO (left) and MRO (right). The dashed line indicates the cutoff score, below which two clusters are considered as identical. The clusters are extracted from the inherent structures of $T = 0.26$ glasses. For the MRO cluster, the cutoff score is slightly increased. The structures of the SRO and MRO templates are presented in the insets.

while the corresponding proportion for hard particles is about 60%. Besides the SRO, 4% (25%) of the soft (hard) particles also develop the MRO. These findings suggest that the soft particles essentially have liquidlike local structures, where some SRO can be developed, but barely any MRO. As for the hard particles, most of them have well-defined SRO, some of which even develop the MRO. In this sense, the soft particles are indeed defects in glasses [1,11,15,37,39]. Compared to previous studies, our work makes a stride further by showing that the local structures of the soft particles are essentially disordered [5,24]. We show in the Supplemental Material [42] that the soft particles indeed contribute to the unstable modes, hence further verifying their defective nature [10]. The disordered nature of soft particles can also be seen from Figs. 3(c) and 3(d). The softest particles frequently break the nearest neighbor cages, indicating their local structures cannot be simply attributed to certain SRO. The disordered local packing of very soft particles cannot completely fill the soft region without residual strain (see Fig. 4), which would drive the softest particles to hop reversibly.

The physical nature of the soft particles observed in the KA model glass system are also explored for two real amorphous systems [64]: a strong glass-forming system ($Cu_{64}Zr_{36}$) [65] and a marginal glass-forming system ($Ni_{64}Zr_{36}$) [66]. We perform similar analyses for the two systems. The soft particles are observed to actively undergo reversible motions with the amplitudes much larger than the averages in the corresponding systems, as shown in Fig. S7 in the Supplemental Material [42], suggesting that these findings can generally be applied to other amorphous solids.

IV. SUMMARY

In summary, a new atomic softness parameter combining both in-cage vibration and nearest neighbor cage-breaking relaxation is proposed, which can probe the dynamics heterogeneities over a longer timescale than that of LDWF. The soft particles identified using our softness parameter are consistent with those from the normal mode analyses. The clear connection between the atomic softness and the real space motions reveals the physical meaning of atomic softness: the ability to rearrange, but not necessarily irreversibly. The softest particles are confined within a rigid wall formed by hard particles, which exhibit strong harmonic vibrations without rearrangement. Therefore, the relaxations of soft particles do not change the distribution of soft regions. We further show that the local environments of soft particles are essentially disordered. The stretched and disordered nature of the very soft particles keep them hopping reversibly, without breaking the larger cage formed by the hard particles.

ACKNOWLEDGMENTS

Work at SUSTech was supported by the National Natural Science Foundation of China under Grant No. 11774142 and the Shenzhen Basic Research Fund under Grant No. JCYJ20180504165817769. The computer time was supported by the Center for Computational Science and Engineering of Southern University of Science and Technology. Work at Ames Laboratory was supported by the U.S. Department of Energy (DOE), Office of Science, Basic Energy Sciences, Materials Science and Engineering Division including a grant of computer time at the National Energy Research Scientific Computing Center (NERSC) in Berkeley, CA. Ames Laboratory is operated for the U.S. DOE by Iowa State University under Contract No. DE-AC02-07CH11358.

[1] H. W. Sheng, E. Ma, and M. J. Kramer, JOM **64**, 856 (2012).
[2] Z. Wang and W.-H. Wang, Natl. Sci. Rev. **6**, 304 (2019).
[3] F. Spaepen, Acta. Metall. **25**, 407 (1977).
[4] J. M. Rieser, C. P. Goodrich, A. J. Liu, and D. J. Durian, Phys. Rev. Lett. **116**, 088001 (2016).
[5] J. Ding, S. Patinet, M. L. Falk, Y. Cheng, and E. Ma, Proc. Natl. Acad. Sci. USA **111**, 14052 (2014).
[6] B. Doliwa and A. Heuer, Phys. Rev. E **67**, 031506 (2003).
[7] A. Heuer, J. Phys.: Condens Matter **20**, 373101 (2008).
[8] Q. Wang, J. Ding, L. Zhang, E. Podryabinkin, A. Shapeev, and E. Ma, npj Comput. Mater. **6**, 194 (2020).
[9] Y. Fan, T. Iwashita, and T. Egami, Nat. Commun. **5**, 5083 (2014).
[10] M. Shimada, D. Coslovich, H. Mizuno, and A. Ikeda, SciPost. Phys. **10**, 001 (2021).

[11] E. D. Cubuk, S. S. Schoenholz, J. M. Rieser, B. D. Malone, J. Rottler, D. J. Durian, E. Kaxiras, and A. J. Liu, Phys. Rev. Lett. **114**, 108001 (2015).

[12] Q. Wang and A. Jain, Nat. Commun. **10**, 5537 (2019).

[13] Z. Fan and E. Ma, Nat. Commun. **12**, 1506 (2021).

[14] N. Xu, V. Vitelli, A. J. Liu, and S. R. Nagel, Europhys. Lett. **90**, 56001 (2010).

[15] M. L. Manning and A. J. Liu, Phys. Rev. Lett. **107**, 108302 (2011).

[16] H. R. Schober and G. Ruocco, Philos. Mag. **84**, 1361 (2004).

[17] D. Richard, M. Ozawa, S. Patinet, E. Stanifer, B. Shang, S. A. Ridout, B. Xu, G. Zhang, P. K. Morse, J. L. Barrat *et al.*, Phys. Rev. Mater. **4**, 113609 (2020).

[18] J. Ding, Y. Q. Cheng, H. Sheng, M. Asta, R. O. Ritchie, and E. Ma, Nat. Commun. **7**, 13733 (2016).

[19] A. Widmer-Cooper, H. Perry, P. Harrowell, and D. R. Reichman, Nat. Phys. **4**, 711 (2008).

[20] L. Wang, A. Ninarello, P. Guan, L. Berthier, G. Szamel, and E. Flenner, Nat. Commun. **10**, 26 (2019).

[21] A. Widmer-Cooper, H. Perry, P. Harrowell, and D. R. Reichman, J. Chem. Phys. **131**, 194508 (2009).

[22] M. Mosayebi, P. Ilg, A. Widmer-Cooper, and E. Del Gado, Phys. Rev. Lett. **112**, 105503 (2014).

[23] S. S. Schoenholz, A. J. Liu, R. A. Riggleman, and J. Rottler, Phys. Rev. X **4**, 031014 (2014).

[24] B. Wang, L. Liangshun, E. Guo, Y. Su, M. Wang, R. O. Ritchie, F. Dong, L. Wang, J. Guo, and H. Fu, npj Comput. Mater. **4**, 41 (2018).

[25] D. Wei, J. Yang, M.-Q. Jiang, B.-C. Wei, Y.-J. Wang, and L.-H. Dai, Phys. Rev. B **99**, 014115 (2019).

[26] B. B. Laird and H. R. Schober, Phys. Rev. Lett. **66**, 636 (1991).

[27] H. Mizuno, M. Shimada, and A. Ikeda, Phys. Rev. Research **2**, 013215 (2020).

[28] B. B. Fan, K. K. Han, H. P. Zhang, and M. Z. Li, J. Non.-Cryst. Solids **540**, 120072 (2020).

[29] A. Widmer-Cooper and P. Harrowell, Phys. Rev. Lett. **96**, 185701 (2006).

[30] W. Kob and H. C. Andersen, Phys. Rev. E **51**, 4626 (1995).

[31] X. Fan, Y. Sun, C.-Z. Wang, K.-M. Ho, M. S. Altman, and L. Huang, Phys. Rev. B **101**, 214104 (2020).

[32] M. Shimada, H. Mizuno, and A. Ikeda, Phys. Rev. E **97**, 022609 (2018).

[33] http://lammps.sandia.gov/.

[34] J. M. Dickey and A. Paskin, Phys. Rev. **188**, 1407 (1969).

[35] A. Rahman, M. J. Mandell, and J. P. McTague, J. Chem. Phys. **64**, 1564 (1976).

[36] X. Tan, Y. Guo, D. Huang, and L. Zhang, Soft Matter **17**, 1330 (2021).

[37] H. Shintani and H. Tanaka, Nat. Mater. **7**, 870 (2008).

[38] M. Guerdane and H. Teichler, Phys. Rev. Lett. **101**, 065506 (2008).

[39] N. Jakse, A. Nassour, and A. Pasturel, Phys. Rev. B **85**, 174201 (2012).

[40] H. P. Zhang, B. B. Fan, J. Q. Wu, W. H. Wang, and M. Z. Li, Phys. Rev. Mater. **4**, 095603 (2020).

[41] H. Zhang, X. Wang, H. B. Yu, and J. F. Douglas, J. Chem. Phys. **154**, 084505 (2021).

[42] See Supplemental Material at http://link.aps.org/supplemental/10.1103/PhysRevB.105.104112 for more details on obtaining the MD-VDOS, the effect of phonons, the relationship between unstable modes and soft particles, the MSD comparison for different cutoffs, the distribution of pairwise alignment score, and the preliminary results for two real amorphous systems ($Cu_{64}Zr_{36}$ and $Ni_{64}Zr_{36}$).

[43] P. Das, V. Ilyin, and I. Procaccia, Phys. Rev. E **100**, 062103 (2019).

[44] P. Das and I. Procaccia, Phys. Rev. Lett. **126**, 085502 (2021).

[45] E. Lerner, G. During, and E. Bouchbinder, Phys. Rev. Lett. **117**, 035501 (2016).

[46] S. Bonfanti, R. Guerra, C. Mondal, I. Procaccia, and S. Zapperi, Phys. Rev. Lett. **125**, 085501 (2020).

[47] H. Mizuno, H. Shiba, and A. Ikeda, Proc. Natl. Acad. Sci. U. S. A. **114**, E9767 (2017).

[48] D. Caprion and H. R. Schober, J. Chem. Phys. **114**, 3236 (2001).

[49] G. Kapteijns, D. Richard, and E. Lerner, Phys. Rev. E **101**, 032130 (2020).

[50] L. Gartner and E. Lerner, SciPost Phys. **1**, 016 (2016).

[51] H. Tong and N. Xu, Phys. Rev. E **90**, 010401(R) (2014).

[52] A. Tanguy, B. Mantisi, and M. Tsamados, Europhys. Lett. **90**, 16004 (2010).

[53] F. H. Stillinger and T. A. Weber, Science **225**, 983 (1984).

[54] R. Pastore, A. Coniglio, and M. P. Ciamarra, Soft Matter **10**, 5724 (2014).

[55] M. P. Ciamarra, R. Pastore, and A. Coniglio, Soft Matter **12**, 358 (2016).

[56] R. Pastore, G. Pesce, A. Sasso, and M. Pica Ciamarra, J. Phys. Chem. Lett. **8**, 1562 (2017).

[57] H. Mizuno, H. Tong, A. Ikeda, and S. Mossa, J. Chem. Phys. **153**, 154501 (2020).

[58] B. Wang, L. J. Wang, B. S. Shang, X. Q. Gao, Y. Yang, H. Y. Bai, M. X. Pan, W. H. Wang, and P. F. Guan, Acta Mater. **195**, 611 (2020).

[59] A. Widmer-Cooper, P. Harrowell, and H. Fynewever, Phys. Rev. Lett. **93**, 135701 (2004).

[60] X. W. Fang, C. Z. Wang, Y. X. Yao, Z. J. Ding, and K. M. Ho, Phys. Rev. B **82**, 184204 (2010).

[61] Y. Sun, F. Zhang, Z. Ye, Y. Zhang, X. W. Fang, Z. J. Ding, C. W. Wang, M. I. Mendelev, R. T. Ott, M. J. Kramer, and K. M. Ho, Sci. Rep. **6**, 23734 (2016).

[62] L. Huang, C. Z. Wang, S. G. Hao, M. J. Kramer, and K. M. Ho, Phys. Rev. B **81**, 094118 (2010).

[63] L. Huang, X. W. Fang, C. Z. Wang, M. J. Kramer, Z. J. Ding, and K. M. Ho, Appl. Phys. Lett. **98**, 231906 (2011).

[64] B. A. Klumov, R. E. Ryltsev, and N. M. Chtchelkatchev, J. Chem. Phys. **149**, 134501 (2018).

[65] M. I. Mendelev, Y. Sun, F. Zhang, C. Z. Wang, and K. M. Ho, J. Chem. Phys. **151**, 214502 (2019).

[66] S. R. Wilson and M. I. Mendelev, Philos. Mag. **95**, 224 (2015).